Available online at www.sciencedirect.com
SCIENCE DIRECT
Catalysis Today 113 (2006) 157–165
CATALYSIS TODAY
www.elsevier.com/locate/cattod

Ni–Ce intermetallic phases in CeO_2-supported nickel catalysts synthesized by γ-radiolysis

S. Chettibi [a], R. Wojcieszak [b], E.H. Boudjennad [a], J. Belloni [c], M.M. Bettahar [b], N. Keghouche [a,*]

[a] *Laboratoire Microstructures et Défauts, Université Mentouri-Constantine, Route de Ain El Bey, 25 110 Constantine, Algeria*
[b] *Laboratoire de Catalyse Hétérogène, UMR 7565, Université Henri Poincaré, Nancy 1, 54506 Vandoeuvre-lès-Nancy, France*
[c] *Laboratoire de Chimie Physique, UMR CNRS/UPS 8000, ELYSE, Université Paris-Sud, Bât. 349, 91405 Orsay, France*

Available online 18 January 2006

Abstract

This work concerns the study of nickel clusters synthesized by radiation-induced reduction of Ni^{2+} ions previously adsorbed on ceria by ionic exchange in the aim to test their performance in catalytic hydrogenation. The nickel catalyst and CeO_2 support were characterized by SEM coupled to X analysis, XRD, H_2-adsorption and H-TPD. The catalyst prepared by irradiation presents high reducibility, dispersion and homogeneity of the metal phase. It is shown that the CeO_2 support stores hydrogen during the radiolytic reduction of Ni ions and that the adsorbed hydrogen amounts strongly increase in the presence of nickel. The catalyst displays high catalytic performance in the benzene hydrogenation reaction (total conversion in a large and low temperature range). These properties are assigned to the high dispersion of nickel and to the promoter role of the support: actually, after the catalytic test, intermetallic nickel–cerium compounds (CeNi and $CeNi_2$) are detected in the sample in addition to the Ni^0 phase.
© 2005 Elsevier B.V. All rights reserved.

Keywords: Ni/CeO_2; Ni–Ce intermetallic phases; Catalyst; Clusters; Radiolysis; Benzene hydrogenation

1. Introduction

Nanosized particles are extensively studied because of their large potential applications. Matter in ultra-divided state has indeed specific properties due to its quasi-atomic state [1,2]. The aggregates of a few atoms are much more easily oxidized than the bulk metal and can be corroded as soon as they are formed. This specific property improves the activity of small metal particles but also makes their stabilization more difficult. Non-noble metals such as nickel, cooper and iron are still more difficult than noble metals to be synthesized at the atomic or oligomeric states [3,4]. Nevertheless, nickel nanoparticles were produced using different methods such as: chemical reduction with hydrazine or alcohol in water solution [4–6], electrochemical reduction [7], sonochemical method [8], microemulsion technique [9] or sol–gel method [10]. As an alternative way, the radiolysis has been proven to be a powerful tool to produce dispersed and monosized metal clusters [1]. Using irradiation, nickel particles have been synthesized in the colloidal state [3] or supported on α-alumina [11]. The radiation-induced reduction of metal ions is achieved by solvated electrons and reducing radicals generated from the solvent and by electrons generated from the support, both having a strong reducing power [11].

The support ceria, a stable fluorite-type oxide, has been extensively studied because of its interesting redox and high dispersive properties [12–14]. Ceria is able to change reversibly from Ce^{IV} under oxidizing conditions to Ce^{III} under reducing conditions. Oxygen atoms in CeO_2 units are very mobile and leave easily the ceria lattice, giving rise to a large variety of non-stoichiometric oxides with the two limiting cases CeO_2 and Ce_2O_3 [13]. Ceria has an insulator behavior in the stoichiometric oxidized state CeO_2 and becomes conductor in the reduced state CeO_{2-x}, acquiring a great capacity to store and to carry oxygen. It was studied in particular in the aim to be used in the automobile emission control system [14,15].

Cerium-based catalysts containing transition metals have attracted increasingly attention in recent years due to their

* Corresponding author. Tel.: +213 31 61 46 14; fax: +213 31 61 46 14.
E-mail address: nassira.keghouche@caramail.com (N. Keghouche).

0920-5861/$ – see front matter © 2005 Elsevier B.V. All rights reserved.
doi:10.1016/j.cattod.2005.11.058

high oxygen storage capability [14–21]. Various studies have shown that the redox properties can be considerably enhanced if additional elements are introduced into the CeO_2 lattice [16,21–28]. Because 4f orbitals give them a surplus of atomic electron valence, rare earth elements can be used to promote the activity and stability of metal catalysts [23]. The beneficial association between species based on nickel and cerium both in oxidized and reduced states have been evidenced [13,22,23]. CeO_2–NiO catalysts have been studied in many hydrogenation reactions [23–26].

The aim of this work is to study Ni/CeO_2 catalysts synthesized by the radiolytic process. After optimizing the adsorption of nickel ions on ceria, the catalyst is irradiated. After the elaboration step, the sample structure is characterized by SEM coupled to X analysis and XRD, whereas its reducibility is determined by temperature programmed reduction (TPR). The metal surface properties are examined by H_2-adsorption and H_2-temperature programmed desorption (TPD). The catalytic activity and stability are tested in the gas phase benzene hydrogenation reaction.

2. Experimental

2.1. Support material and chemical reagents

The solutions are prepared in ultra-pure water of 18 MΩ cm resistivity obtained with alpha Q Millipore apparatus. The reagents are pure chemicals and used as purchased: the ammonium hydroxide NH_4OH is provided by Prolabo, the nickel formate $Ni(HCOO)_2{\cdot}7H_2O$ and the propanol-2 $(CH_3)_2CHOH$ by Merck. The support material CeO_2, was purchased from Rhône Poulenc. Its isoelectric point is at around pH 6.7.

2.2. Sample preparation

The catalyst preparation was carried out as reported in Ref. [11]. Nickel ions were adsorbed by ionic exchange on ceria. The support sample, constituted of 200 mg of cerium oxide, initially yellow colored, was impregnated with 8.5 ml of a nickel formate solution 2×10^{-2} mol dm^{-3} (load ratio Ni^{2+}/CeO_2 = 5 wt.% or a total amount of Ni^{2+} ions of 8×10^{-4} mol g_{cat}^{-1}) and 0.2 mol dm^{-3} 2-propanol in order to ensure reducing conditions under irradiation. The supernatant solution was alkalinized with ammonium hydroxide until reaching pH_i 11 corresponding to the formation of the stable nickel hexamine complex $[Ni(NH_3)_6]^{2+}$ characterized by the UV absorption (λ = 364 nm). The support was then in contact under stirring for 24 h at room temperature with the impregnation solution containing the nickel precursor. During this adsorption step, the nickel content of the supernatant solution decreases during the early hours and becomes stable after 24 h. Simultaneously, the pH of the solution decreases from the initial pH_i to a final pH_f 8.4. At the end, ceria acquires a green color.

2.3. Irradiation

Then, the sample was purged under nitrogen flow (during 15–20 min) and irradiated. The irradiation was carried out using a ^{60}Co γ-source at a dose rate of 5 kGy h^{-1} with a total dose of 92 kGy. This dose has been chosen because it is able to reduce all Ni^{2+} ions in a free solution according to a mean radiolytic yield of $G = 2 \times 10^{-7}$ mol J^{-1} [3]. (The rest of the total reduction yield, which is equal to 2×10^{-7} mol J^{-1}, produces mostly H_2, because Ni atoms are easily corroded by water). However, on one hand the ions fixed on the support are locally more concentrated, so the dose required could be higher, and on the other hand, the support provides under irradiation supplementary electrons which also contribute to reduction [11]. The holes generated in ceria react with 2-propanol or formate at the water interface and yield also secondary reducing radicals. The absorbed dose is possibly used to reduce CeO_2 into Ce_2O_3 directly or indirectly by electron transfer from Ni^0 to ceria. The irradiated sample was then filtered and dried still under nitrogen flow. The deposits obtained after drying were grey. At this step, the catalyst is ready for catalysis.

2.4. Characterization

X-ray diffraction spectra were recorded on a powder diffractometer Siemens D8, using the Kα line of copper (λ = 0.154 nm, intensity = 20 mA and voltage = 40 kV). The various phases constituting the catalyst were identified using the ASTM files. The catalyst is dispersed on an adhesive tape. In spite of the high resolution of this apparatus, only the most intense peaks of the phases containing nickel appear on the spectra. Due to the low proportion of nickel compared to ceria, the other peaks are indeed under the detection threshold. In the aim to increase the resolution, long time exposure was applied.

A scanning electron microscope (SEM) Tescan Vega (TS 5130 MM type), coupled to a Rönteg Edwin NT system, was used for the visualization and the energy dispersive spectroscopy (EDS) microanalysis of the samples. For microscopic imaging and EDS analysis, the samples are dispersed on an adhesive carbon pastille. To avoid the charge effects due to unconducting ceria, a thin gold film is evaporated on the samples. The proportion of the chemical elements was determined using the Rönteg Edwin Wintools program. The coupling of both techniques, SEM and EDS analysis, gives information about the homogeneity of the metal distribution on the support.

The gases were purchased from Air Liquide. Oxygen traces were eliminated from argon (99.995%) and hydrogen (99.995%) by using a manganese oxytrap (Engelhardt). Chemisorption and thermal treatments were performed with a sample of 50 mg in a pulse chromatographic microreactor, equipped with the catharometric detector microchromatograph (ATM 200, Hewlett Packard), fitted with molecular sieve columns and MTI software. Thermal treatment of the sample was carried out with a flow rate of 10 °C min^{-1} up to 350 °C during 45 min with pure H_2.

For H_2-chemisorption studies at room temperature, the catalyst was flowed under argon for 2 h, and cooled down to

room temperature. Then the reactant gas (100 ppm H_2/argon) was injected in the reactor every 2 min. The amount of H_2 adsorbed is used to calculate the accessibility to the metal surface sites, defined as the ratio between the number of H_2 molecules adsorbed and the total number of nickel atoms.

The subsequent H_2-TPD measurement was performed after the adsorption step above and a purge with argon at room temperature for 1 h. The amount of H_2 desorbed is measured when the system is heated at a rate of 5 °C min^{-1} up to 700 °C under argon flow (flow rate = 100 cm^3 min^{-1}). The desorbed hydrogen is detected with a thermal conductivity detector in an Agilent G2890A chromatograph. The amount of H_2 desorbed is calculated by integrating the TPD curves. This amount indicates the metal dispersion as reported in Ref. [21].

The H_2-TPR study was carried out on a sample (50 mg) placed in a quartz tube and treated first in a flow of argon at room temperature for 1 h. Then, using a H_2/Ar (1000 ppm) mixture as the reducing agent (flow rate = 90 cm^3 min^{-1}), it was heated at a rate of 5 °C min^{-1} up to 800 °C. The TPR measurements of H_2 consumed can provide a view of low and high temperature interactions between H_2 and the catalyst.

In addition, the TPR method gives information about the catalyst redox behavior. The degree of reduction was determined according to Ref. [21]. The sample was heated first at a rate of 10 °C min^{-1} up to 300 °C for 45 min in a flow of pure hydrogen (flow rate = 50 cm^3 min^{-1}). After the reduction, the sample was treated in an argon flow at 350 °C for 1 h with a flow rate of 100 cm^3 min^{-1} in order to desorb the hydrogen gas, which has not been used for reduction and to calculate, by difference with the initial amount of H_2 in the flow, the reduction equivalent of the catalyst.

2.5. Catalytic test

The performances of the catalyst were tested in the benzene hydrogenation reaction, converting, under H_2 flow, benzene to cyclohexane ($C_6H_6 + 3\,H_2 \rightarrow C_6H_{12}$). This test was carried out at atmospheric pressure, in a quartz fixed-bed reactor equipped with a thermocouple, on which was deposited 50 mg of the catalyst charge. Note that two types of tests had been performed: in the first one, the sample obtained after irradiation, was not previously submitted to temperature treatment under hydrogen atmosphere. In the second one, the catalyst was treated (see above). The reactant mixture containing benzene and H_2 (benzene/H_2 = 1 vol.%) was prepared by flowing the H_2 stream through benzene (Merck, >99%) placed in a saturator maintained at 5.4 °C. The mixture was then passed through the reactor with a total flow rate of 50 cm^3 min^{-1}. The catalytic test was carried out at various temperatures on the same catalyst sample. The sample was heated or cooled at a rate of 10 °C min^{-1}. Benzene and the reaction products were analyzed each 15 min with 5730A Hewlett Packard gas chromatograph, operated at a programmed temperature with a flame ionization detector (FID). The catalyst activity has been evaluated when the steady state was reached.

3. Results and discussion

3.1. TPR-H_2 profiles

First, the TPR spectrum of the irradiated support CeO_2, in the absence of nickel, was recorded (dose = 3.2 kGy, dose rate = 5 kGy h^{-1}) (Fig. 1a and Table 1). This profile presents two peaks at 500 and 700 °C, which are due to the reduction of CeO_2 into Ce_2O_3 [15] (total amount of H_2 consumed $\approx 8 \times 10^{-4}$ mol g_{cat}^{-1}). The reduction occurs first at the surface (oxygen in a tetrahedral coordination site, bonded to one Ce^{IV}), then progressively in the bulk [14,15,22]. Thus the lowest temperature peak is assigned to the easily reducible surface oxygen of CeO_2, while the high temperature peak, at 700 °C, results from the removal of the bulk oxygen [14]. Even though the profile of irradiated ceria is similar to that of non-irradiated CeO_2 reported in the literature [14,15,17], it presents two main differences: on one hand, the relative intensity of the first peak is more important; on the other hand, the second peak is shifted to a lower temperature ($\Delta T \approx 130$ °C), indicating, for the irradiated ceria, a larger fraction of surface oxygen atoms and an easier H_2 chemisorption, probably due to higher porosity.

The TPR profile of the irradiated nickel catalyst (Ni/CeO_2 ratio = 5 wt.%, dose = 92 kGy and dose rate = 5 kGy h^{-1}), shown in Fig. 1b, presents two temperature maxima. The first

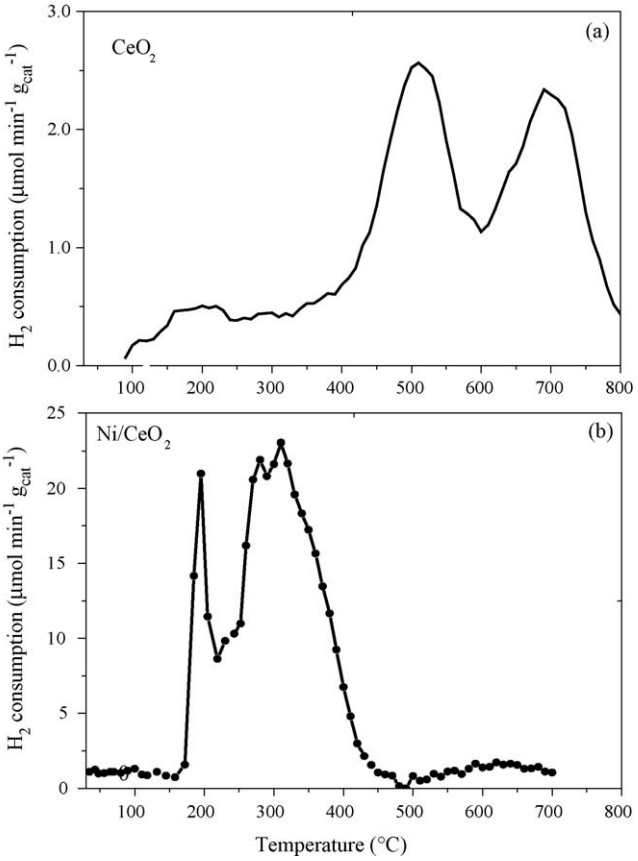

Fig. 1. TPR-H_2 profiles. (a) CeO_2 support after irradiation (dose = 3.2 kGy and dose rate = 5 kGy h^{-1}). (b) Catalyst Ni/CeO_2 5 wt.% after irradiation (dose = 92 kGy and dose rate = 5 kGy h^{-1}).

Table 1
Surface properties and reducibility of CeO_2 support and Ni/CeO_2 catalyst

Material	TPR H_2 consumed (10^{-4} mol g_{cat}^{-1})	H_2 adsorbed (10^{-4} mol g_{cat}^{-1}) at RT	TPD H_2 desorbed (10^{-4} mol g_{cat}^{-1}) (temperature maximum (°C))
CeO_2			
Non-irradiated	–	0	0.53 (420, 580)
Irradiated (3.2 kGy, 5 kGy h^{-1})	0.80	0	1.51 (420, 580)
Irradiated then treated under H_2/350 °C	–	–	1.86 (380, 450–600)
Ni/CeO_2			
Non-irradiated	–	0	–
Irradiated (92 kGy, 5 kGy h^{-1})	8	0	7.84 (300, 400, 500, 600)
Irradiated then treated under H_2/350 °C	–	0.68	1.46 (250)

one is located at 195 °C and the second close to 300 °C (none in the range 500–700 °C). In the literature, Ni/CeO_2 catalysts prepared by calcination/H_2-reduction exhibit also two TPR peaks. However, the first peak at 195 °C of radiolytic catalyst is at markedly lower temperature than the values reported in the literature for not irradiated [29], unsupported or ceria-supported NiO [30]. The second peak around 300 °C is also slightly shifted to a lower temperature than in the literature. It is generally assigned to the two-step reduction of NiO, in still stronger interaction with ceria, into Ni^0. It means that H_2 is interacting with two different sites of the catalyst. The first type at 195 °C is a tight bonding site on the radiolytic catalyst. Nickel and cerium were probably, at least partially, reduced during irradiation and these species make easier the further reduction of nickel oxide. The H_2 consumption in the first peak is lower than that in the second peak, which suggests that NiO could be reduced mostly during the second step. The peak at 300 °C can also result from the partial reduction of CeO_2 oxide, which can occur at lower temperature than for ceria alone (and not at 500–700 °C) due to the promoter role of nickel particles [31–33].

It is noteworthy, that the peak intensity in Fig. 1b is much higher (by a factor of 10) than in Fig. 1a without Ni, though the nickel amount in the catalyst is only 5% of CeO_2. Indeed, after irradiation, the integration of the curve in Fig. 1b indicates that the consumption of H_2 corresponds to a total amount for both peaks of 8×10^{-4} mol (H_2) g_{cat}^{-1} (Table 1).

3.2. H_2-desorption and chemisorption

The sorption behavior of the support ceria without irradiation was studied under the same conditions as the nickel catalyst supported on non-irradiated or irradiated ceria, before and after H_2 treatment at 350 °C (Table 1).

3.2.1. Support

The adsorption experiments at room temperature show that, whatever is the state of CeO_2 (irradiated or not and treated under H_2 or not), the support CeO_2 does not adsorb hydrogen. On the contrary, the TPD study shows that the as-received support desorbs small amounts of hydrogen (0.53×10^{-4} mol g_{cat}^{-1}) (Table 1). After irradiation (dose = 3.2 kGy and dose rate = 5 kGy h^{-1}), this amount increases and it is three and 3.6 times greater before and after H_2 treatment, respectively. The TPD profiles of the non-irradiated and of the irradiated ceria present two intense temperature H_2-desorption peaks at 400 and 600 °C (Fig. 2a and b, respectively). After the subsequent H_2 treatment (Fig. 2c), the first peak is shifted towards a lower temperature whereas the second peak width increases. The TPD profile of the non-irradiated ceria (Fig. 2a) and the desorbed H_2 amount are in agreement with previous studies, where maximum values of hydrogen desorbed from ceria have been obtained after reduction at 400 and 600 °C [30]. The peaks observed can be attributed to two types of CeO_2–H_2 bond breaking: H_2 adsorption bonds dissociate at high temperature and possibly the adsorption site number decreases due to surface dehydroxylation. The enhancement of desorbed hydrogen after irradiation (Fig. 2b) originates from the radiolysis and agrees with other studies where it has been shown that

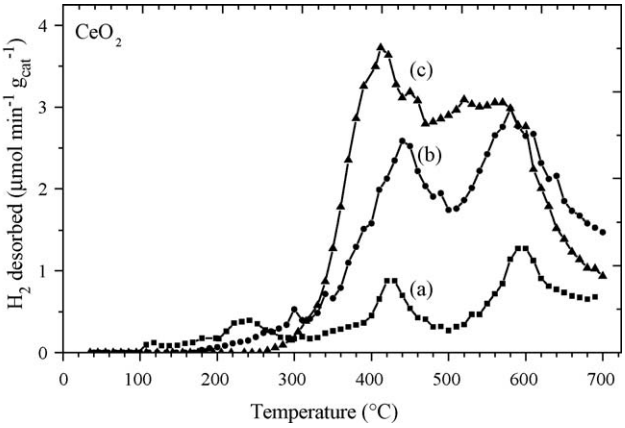

Fig. 2. TPD profile of the CeO_2 support. (a) Before irradiation and treatment. (b) After irradiation (dose = 3.2 kGy, dose rate = 5 kGy h^{-1}). (c) After H_2 treatment at 350 °C during 45 min following the irradiation.

irradiation of ceria in the presence of water produces hydrogen [34]. For comparison, whereas the sample non-H_2-treated, desorbed around 1.50×10^{-4} mol g_{cat}^{-1}, the H_2 amount desorbed in the pretreated sample is now 1.85×10^{-4} mol g_{cat}^{-1} (Fig. 2c, Table 1). This corresponds to the total H_2 adsorption capacity of the irradiated support. It is known indeed that alumina heated up to 400 °C in H_2 for several hours is able to adsorb hydrogen [32]. The neat support acts thus as a hydrogen reservoir, the level of which depends on the pre-treatment.

3.2.2. *Ni/CeO₂ catalyst*

The irradiated catalyst containing nickel desorbs reversibly greater amounts of hydrogen (7.84×10^{-4} mol g_{cat}^{-1}) than the support alone (Table 1). The amount corresponds to almost the same amount as hydrogen consumption during H_2 treatment (8×10^{-4} mol g_{cat}^{-1}). This corresponds to the total H_2 adsorption capacity of the Ni/CeO_2 sample. The presence of nickel on the support increases markedly the hydrogen reservoir capacity of the catalyst. Since NiO does not adsorb hydrogen, the amount of H_2 adsorded is due to reduced Ni^0.

First, the amount of H_2 desorbed originates only from radiolysis. Therefore, this demonstrates that the nickel part of the catalyst desorbs about $(7.8-1.5) \times 10^{-4} = 6.3 \times 10^{-4}$ mol g_{cat}^{-1} in addition to the irradiated support, (initial Ni^{2+} was 8×10^{-4} mol g_{cat}^{-1}). Assuming that one H_2 molecule is adsorbed per Ni atom, the accessible specific area of the catalyst is 106 m^2 g_{Ni}^{-1}.

On the other hand, the irradiated catalyst exhibits a complex temperature profile: a main peak at around 300 °C and another broad and almost flat band in the range 400–600 °C (Fig. 3). The decomposition of the profile suggests that this latter section is constituted of at least three peaks (at approximately 400, 500 and 600 °C). The peak at 300 °C is higher than usually in other studies without irradiation [15]. It may be ascribed to hydrogen adsorbed on nickel sites. As to the three high temperature peaks, they are tentatively assigned to hydrogen adsorbed on the support or on the metal-support compounds, because they are more similar to the profile of Fig. 2. This part of species, which was first dissociated probably arises from the hydrogen spill-over [35,36], namely hydrogen which was first dissociated on nickel nanoparticles produced during the irradiation process, and then migrates from the metal to the oxide surface.

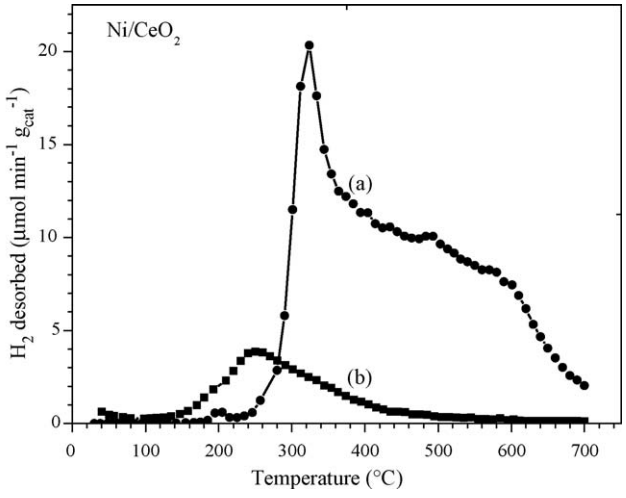

Fig. 3. TPD profile of the catalyst Ni/CeO_2 5 wt.%. (a) After irradiation (dose = 92 kGy and dose rate = 5 kGy h^{-1}). (b) After H_2 treatment at 350 °C during 45 min following the irradiation.

3.2.3. *H_2 pretreated Ni/CeO₂ catalyst*

In contrast, the sample Ni/CeO_2 irradiated, then thermally treated at 350 °C under a hydrogen flow, adsorbs at room temperature 0.68×10^{-4} mol g_{cat}^{-1} only, and desorbs higher amounts of hydrogen (1.85×10^{-4} mol g_{cat}^{-1}) as it can be seen in Table 1. Remarkably, the amounts of desorbed hydrogen are lower than those obtained for the irradiated and non-treated catalyst (Table 1). In addition, the TPD profile exhibits only a single peak, less intense and at a lower temperature (250 °C) (Fig. 3b). This peak is ascribed to hydrogen molecules less tightly bonded to the metal phase. High temperature peaks are not observed for the irradiated and non-treated catalyst (Fig. 3b), because H_2 amounts already desorbed during the 350 °C treatment (Table 1). In other words, the heat treatment both reduces the irradiated sample and removes the surface H_2 molecules produced and adsorbed during the radiolytic synthesis. This induces new nickel sites active for hydrogen adsorption.

When the sample was pretreated under H_2 at 350 °C, the adsorbed and desorbed amounts are less than without treatment (Table 1), because the less bounded H_2 molecules are not taken into account. The part of strongly adsorbed molecules is about 20% of the total.

3.3. *Benzene hydrogenation*

The activity of the catalyst Ni/CeO_2 synthesized by radiolytic process was tested in the benzene hydrogenation as a function of the reaction temperature in the range 75–225 °C (Fig. 4a and b) and of a H_2 pretreatment (Fig. 4c). In order to study the conditions of catalyst efficiency and deactivation, the reaction temperature was gradually increased up to 225 °C (Fig. 4a–c), and then decreased to 75 °C (Fig. 4b).

The catalytic test of the CeO_2 support alone, under the same reaction conditions as for Ni/CeO_2, showed that the support is inactive in the benzene hydrogenation. With the Ni/CeO_2 catalyst, only cyclohexane is detected as a reaction product in the exit gas.

When increasing the temperature reaction of the irradiated and non-H_2-pretreated catalyst (Fig. 4a), the benzene conversion takes place at a remarkably low temperature, around 100 °C. It is total above 175 °C, then constant at least up to 240 °C. Moreover, in the deceasing temperature sequence (Fig. 4b), the catalyst activity is total in a large temperature range (225–100 °C) and is still 60% at 75 °C. The stability test at 100 °C (point A in the decreasing sequence of Fig. 4b), shows that it is stable with time on stream at least for 20 h (inset Fig. 4).

The conversion rate obtained when the catalyst is H_2-pretreated at 350 °C after irradiation (Fig. 4c) is intermediate

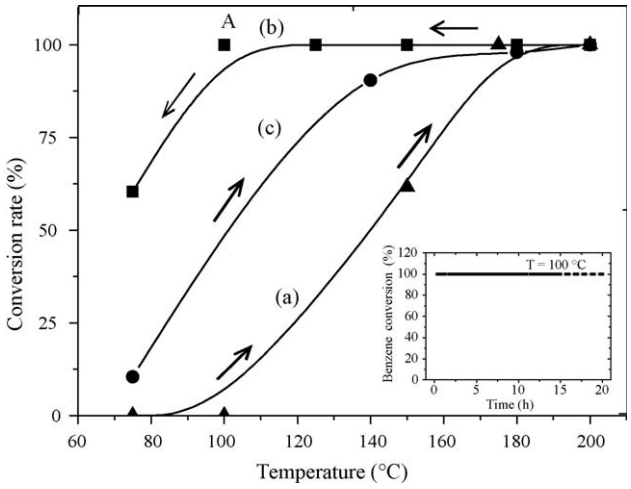

Fig. 4. Benzene conversion rate over the catalyst Ni/CeO_2 5 wt.% (dose = 92 kGy and dose rate = 5 kGy h^{-1}). (a) Fresh catalyst at the increasing-temperature range from 75 to 225 °C then (b) at the decreasing-temperature from 225 to 75 °C. (c) Catalyst treated at 350 °C during 45 min following the irradiation at the increasing temperature range. Reactant flow rate = 50 - cm^3 min^{-1}. Catalyst sample = 50 mg. Inset: conversion versus time of stream at 100 °C over the catalyst at point A.

between those of curves a and b: the conversion rate increases until 75 °C and reaches the maximum value above 140 °C (Fig. 4c).

The fact that the conversion rate in the decreasing-temperature sequence (curve b) is markedly higher than the increasing-temperature sequence (curve a) illustrates that the catalyst is activated during the benzene hydrogenation reaction when the temperature increases. A H_2-pretreatment at 350 °C also enhances somewhat the activity, so that the total conversion is reached at a slightly lower temperature (curve c), but the results are lower than those of the irradiated/non-pretreated sample with only one catalytic cycle up to 225 °C. This seems to indicate that a complementary reduction of the catalyst probably occurs during this step in parallel with the benzene hydrogenation start. However, the remarkable activity at low temperature, without pretreatment, is clearly due for the essential part to the radiation-induced reduction method at room temperature. Note again that electrons and radiolytic radicals, which are generated in the depth of the material CeO_2/adsorbed nickel ions, are very strong reducing agents, and that, contrarily to the H_2 reduction method, heating for the diffusion of H_2 and its dissociation into the reducing H atoms is not necessary. Moreover, sintering is prevented.

The results are in good agreement with the TPR study, which showed that the H_2 consumption on the radiolytic catalyst also occurs at a low temperature range. A close examination of the catalyst TPR profile (Fig. 1b) indicates indeed that, in fact, the consumption begins at about 150 °C and the maximum temperature of the first peak is 195 °C.

In summary, the benzene conversion is total, at least with a 50 ml min^{-1} flow rate and a 50 mg sample, at a relatively low temperature and in a large temperature range. Moreover, it is very stable at 100 °C for at least 20 h. Thus the radiation-induced catalyst appears as particularly efficient.

3.4. Structural study

Fig. 5 presents SEM micrographs of Ni/CeO_2 5 wt.% at several steps of the preparation or of the catalytic test (Fig. 5a after Ni^{2+} adsorption, Fig. 5b after irradiation and Fig. 5c after catalytic test). The size of CeO_2 particles is 1–5 μm. The X analysis was performed on two different ceria grains of the sample (positions 1 and 2 in Fig. 5 b and Table 2). In spite of the low resolution of the SEM to observe the metal aggregates, its coupling with EDS analysis indicates a homogeneous dispersion of the nickel on the surface (Table 2).

In Fig. 6 are reported the XRD spectra of the commercial support (non-H_2-treated and non-irradiated), and of the catalyst Ni/CeO_2 5 wt.% after the catalytic test (up to 225 °C after the increasing-temperature sequence of Fig. 4a). The XRD pattern of the support presents the typical peaks of the ceria in the fluorite structure with a cell parameter $a = 0.540$ nm (Fig. 6a and Table 3). The spectra of the irradiated support and of the catalyst after the irradiation and before the catalytic test are similar to those of the support pattern (Fig. 6a, Table 3). Indeed, none of the peaks corresponding to nickel (Ni^0 or NiO) is detected, probably because the nickel content is small and Ni^0 particles are extremely small.

After the benzene hydrogenation test of the irradiated catalyst, new additional phases are clearly detected in the sample, namely Ni^0, NiCe and NiCe (Fig. 6b and Table 3). Either more nickel ion were reduced during the catalyst test, or the Ni^0 particles have grown during the catalytic test, so favoring their detection. The appearance of diffraction peaks at $2\theta = 44.6$ and 57.6° suggests that nickel is crystallized in hexagonal structure. The next peak, which is expected around 71°, is not observed. It can be hidden by the intense CeO_2 peak situated at 69.6° or it was shifted to a lower value ($2\theta = 68.3°$). In this case the cell is relaxed ($a' = 0.274$ nm instead of 0.265 nm obtained from peaks observed at 44.6° and 57.6°). The 68.3° reflection can also be assigned to (0 2 2) face of NiCe which is characterized by $2\theta = 69.0°$ (ASTM files). This allows us to estimate the c cell parameter of NiCe phase ($c = 0.298$ nm). Note that, on one hand, the relative intensities of these nascent phases are different from that of the bulk as reported on ASTM files. For example, the face (0 2 1) of nickel is more intense than (0 1 1), and the face (1 3 0) of NiCe is observed alone. On the other hand, some reflections such as those arising from (1 1 1), (1 3 1) and (0 0 2) for NiCe and (3 1 1) for Ni_2Ce are not observed. These results indicate that the intermetallic phases NiCe and Ni_2Ce are disordered to some extent. Their low diffraction intensities compared to those of the support indicate that the metal particles have very small sizes. Finally, NiO is not observed, indicating a high reduction degree of nickel in the radiolytic catalyst. This is in agreement with TPR results (see Section 3.1) and benzene hydrogenation tests (Section 3.3).

3.5. Correlation structure-catalytic properties

The behavior of Ni/CeO_2 catalysts is known to be peculiar compared to other oxide-supported catalysts. It has been shown

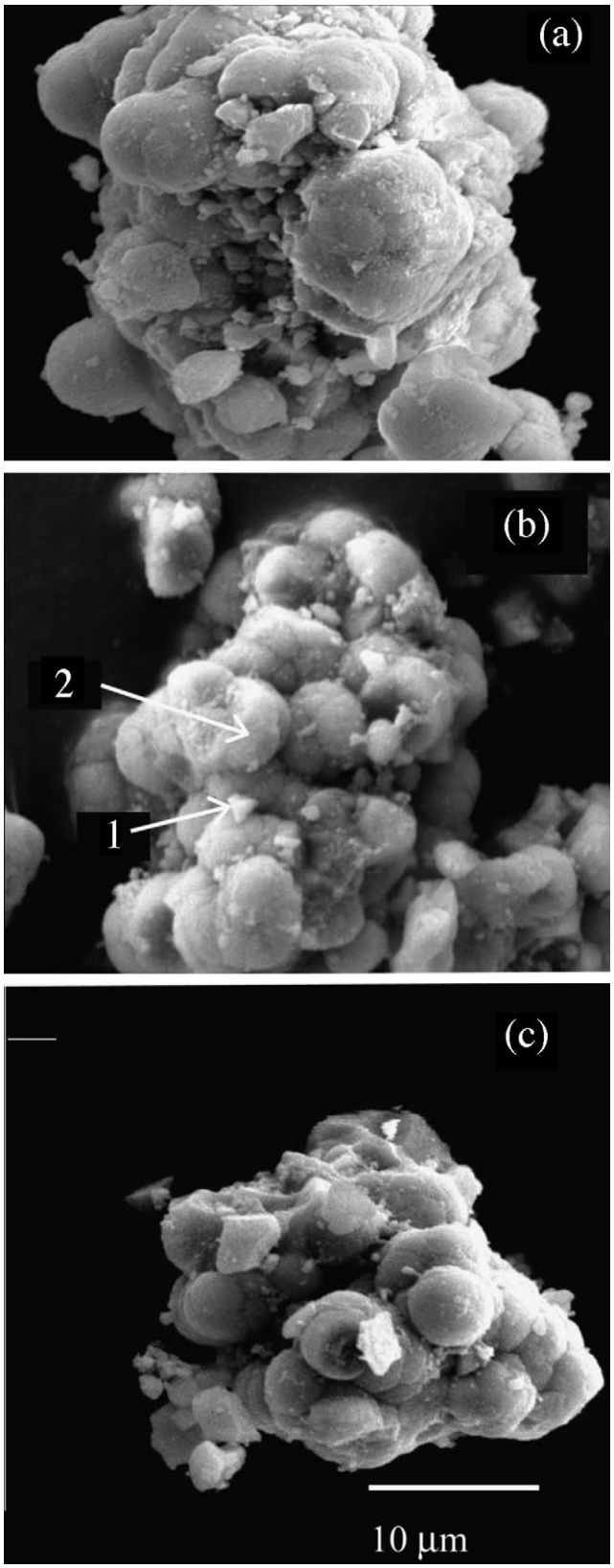

Fig. 5. SEM imaging of Ni/CeO_2. (a) After Ni^{2+} adsorption. (b) After irradiation at a dose = 92 kGy and dose rate = 5 kGy h^{-1}. (c) After catalytic test. Initial conditions: $[Ni^{2+}] = 2 \times 10^{-2}$ mol dm^{-3}, Ni/CeO_2 ratio = 5 wt.%, pH 11.

Table 2
Atomic proportions of Ni, Ce and O in the catalyst Ni 5 wt.%/CeO_2 after irradiation (dose = 92 kGy and dose rate = 5 kGy h^{-1}) and after the catalytic test

Element	Content (at.%)		
	After irradiation		After benzene conversion
	1	2	
O	62.7	62.1	64.3
Ce	34.4	34.9	32.8
Ni	2.9	3.0	2.8
O/Ce	1.82	1.78	1.96

The X element content is [X]/([O] + [Ni] + [Ce]). The two positions 1 and 2 are shown in Fig. 5b.

that they have the lowest reduction temperature and are accordingly activated at a lower temperature, favoring the catalyst stability. Some authors reported the promoter role in the nickel reducibility of some supports such as CeO_2 and, to a lesser extent, TiO_2 and ZrO_2 [12,27,28], favoring the nickel reduction [35]. Indeed, it was demonstrated, in radiolysis studies [3], that nascent nickel atoms have a quite low redox potential and are much fragile to protons. The potential of adsorbed ions on the support increases and thus favors nickel reduction. Romoroson et al. [36] reported the existence of a spill-over effect of hydrogen atoms over Ni/CeO_2 catalysts. The hydrogen dissociates at the nickel surface (Ni^0) and transfers

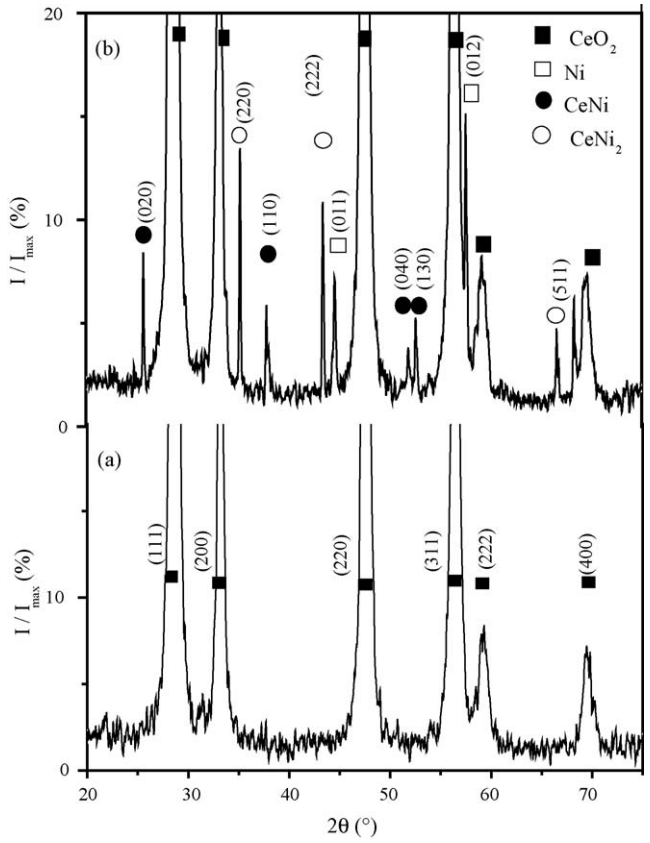

Fig. 6. XRD patterns. (a) Support CeO_2. (b) Catalyst Ni/CeO_2 5 wt.% after the catalytic test.

Table 3
XRD study of CeO_2 and Ni/CeO_2 (5 wt.%, dose = 92 kGy and dose rate = 5 kGy h^{-1})

Sample	Phases	Observed reflections (*h k l*)	Structure	Cell parameters	
				Experimental (nm)	ASTM
Support					
Non-irradiated/after irradiation	CeO_2	(1 1 1), (2 0 0), (2 2 0), (3 1 1), (2 2 2), (4 0 0)	Cubic (fluorite)	$a = 0.540$[a]	$a = 0.541$
Catalyst					
Fresh	CeO_2	(1 1 1), (2 0 0), (2 2 0), (3 1 1), (2 2 2), (4 0 0)	Cubic (fluorite)	$a = 0.540$[a]	$a = 0.541$
After catalytic test	CeO_2	(1 1 1), (2 0 0), (2 2 0), (3 1 1), (2 2 2), (4 0 0)	Cubic (fluorite)	$a = 0.540$[a]	$a = 0.541$
	Ni	(0 1 1), (0 1 2), (1 1 0)	Hexagonal	$a = 0.263$, $b = 0.450$[b], $a' = 0.274$[c]	$a = 0.265$, $b = 0.434$
	CeNi	(0 2 0), (1 1 0), (0 4 0), (1 3 0), (0 2 2)	Orthorhombic (BCr)	$a = 0.242$, $b = 0.704$[d], $c = 0.298$[e]	$a = 0.437$, $b = 1.056$, $c = 0.378$
	$CeNi_2$	(2 2 0), (2 2 0), (5 1 1)	Cubic ($MgCu_2$)	$a = 0.724$[a]	$a = 0.720$

The parameters are calculated from the inter-reticular distance *d* as.
[a] $d^2 = a^2/(h^2 + k^2 + l^2)$ for cubic structure.
[b] $1/d^2 = (h^2 + k^2)/a^2 + l/c^2$ for hexagonal structure using the reflections (0 1 1) and (0 1 2).
[c] $1/d^2 = (h^2 + k^2)/a^2 + l/c^2$ for hexagonal structure using the reflections (1 1 0).
[d] $1/d^2 = h^2/a^2 + k^2/b^2 + l/c^2$ for orthorhombic using the reflections (0 2 0) and (1 1 0).
[e] $1/d^2 = h^2/a^2 + k^2/b^2 + l/c^2$ for orthorhombic using the reflections (0 2 2).

protons to the ceria support, generating new hydroxyl groups. The high activity is explained in this case by the excess of electrons at the metal surface.

During CeO_2 irradiation, creation of (e^-, h^+) pairs occurs. Electrons diffuse to the surface. They cross through the interface to the aqueous phase, where they react with alcohol or formate to produce molecular hydrogen (Section 2.3) and possibly to reduce ceria. After irradiation under reducing conditions, the nickel is reduced and the support itself can be reduced for a small part into CeO_{2-x}. Nickel ions are reduced in situ by radiolytic species, mainly directly by e^- generated from the support or by solvated electrons generated at the water interface [11]. TPD results seem to indicate that after H_2 treatment or/and during the start of the benzene hydrogenation reaction, the catalyst is activated, possibly because the reducing conditions contribute to achieve the reduction of the nickel ions or even produce Ce^{III} sites through an electron transfer from the nickel particles to ceria [36]. These electrons are accepted in the 4f hybrid orbital of cerium.

Several works pointed out to the beneficial association between species based on nickel and cerium [17,25,26,30]. However, the formation of the Ni–Ce intermetallic phases seems to depend in fact strongly on the preparation conditions. The possible generation of Ni–Ce intermetallic compounds at ultra divided state in the Ni/CeO_2 catalysts is not clearly established, whereas generally NiO and $NiCeO_x$ compounds are observed [12,14,15,22]. For example, the EXAFS study of the local structure of Ce and dopant atoms (Fe, Ni) in ZrO_2–CeO_2 systems indicates no solid solution formation for Ni doped oxide [37]. Sohier et al. have shown that the formation of Ni or NiO depends on the Ni/Ce ratio [38].

For catalysts prepared by irradiation-induced reduction as in this study, results of Sections 3.3 and 3.4 demonstrated the promoter role of ceria on nickel reducibility, the clear observation of NiCe and Ni_2Ce intermetallic phases (Fig. 6b, Table 2), together with a remarkable catalytic activity, which seems to confirm the beneficial role of Ni–Ce bonding. These phases are known in materials to be activated indeed at low temperature more quickly than other intermetallic compounds [24], which is supported by our results.

It seems that the benzene conversion obtained at the end of the catalytic test in the decreasing-temperature sequence is optimized by low temperature conditions. In fact, a lower temperature prevents sintering of metal particles and segregation of cerium in Ni–Ce compounds [39].

Then, the irradiation, which was carried out at room temperature favors the stabilization of intermetallic phases, giving a plateau in the conversion curve in a large and low temperature range ($100 < T < 225$ °C). In contrast, in conventional H_2 reduction methods, higher temperature should be required to dissociate H_2, and this is less favorable to intermetallic phase stabilization and benzene hydrogenation.

4. Conclusion

Nickel catalysts prepared by nickel ion adsorption on ceria, then γ-irradiation under wet conditions at room temperature, display a high metal dispersion on the oxide support with a homogeneous repartition. Nickel ions are more easily reduced than NiO. The irradiation preparation method leads to the formation of intermetallic phases NiCe and Ni_2Ce. The catalyst so prepared acquires a quite high hydrogen adsorption capacity and a remarkably important and stable activity in benzene hydrogenation. In particular, under the conditions of the study, the catalyst totally converts benzene to cyclohexane at temperature as low as 100 °C and remains stable for at least 20 h at this temperature. The high catalytic performance of Ni/CeO_2 radiolytic catalyst is attributed to the high dispersion of

nickel and to the promoter role of the support through the formation of Ni–Ce phases.

Acknowledgements

This work has benefited of the aid of the Algerian ''Fond National de la Recherche'' and has been supported by the Comité Mixte d'Evaluation et de Prospective de Coopération Interuniversitaire Franco-Algérienne, (contract 04 MDU 616 University of Constantine/University Paris-Sud XI). The authors are grateful to Michèle Lourseau for irradiation experiments.

References

[1] J. Belloni, M. Mostafavi, H. Remita, J.L. Marignier, M.O. Delcourt, in: J. Bradley, B. Chaudret (Eds. of the special issue) Synthesis, Chemistry, Some Applications of Metal Nanoparticles, New J. Chem. 22 (1998) 1239.
[2] J.H. Fendler (Ed.), Nanoparticles and Nanostructured Films, Wiley, 1998.
[3] J.L. Marignier, J. Belloni, M.-O. Delcourt, J.P. Chevalier, Nature 317 (1985) 344.
[4] D.H. Chen, C.H. Hsieh, J. Mater. Chem. 12 (2002) 2412.
[5] A.G. Boudjahem, S. Monteverdi, M. Mercy, M.M. Bettahar, J. Catal. 221 (2004) 325.
[6] S.H. Wu, D.H. Chen, J. Colloids Interf. Sci. 259 (2003) 282.
[7] M.P. Zach, R.M. Penner, Adv. Mater. 12 (2000) 878.
[8] Y. Mizukoshi, K. Okitsu, Y. Maeda, T.A. Yamamoto, R. Oshima, Y. Nagata, J. Phys. Chem. B 101 (1997) 7033.
[9] K. Osseo-Asare, F.J. Arriagada, Ceram. Trans. 12 (1990) 3.
[10] A. Syukri, T. Ban, Y. Ohya, Y. Takahashi, Mater. Chem. Phys. 78 (2003) 645.
[11] N. Keghouche, S. Chettibi, F. Latrèche, M.M. Bettahar, J. Belloni, J.L. Marignier, Radiat. Phys. Chem. 74 (2005) 185.
[12] T. Zhu, M. Flytzani-Stephanopoulos, Appl. Catal. A: Gen. 208 (2001) 403.
[13] L. Filotti, A. Bensalem, F. Bozon-Verduraz, G.A. Shafeer, V.V. Voronov, Appl. Surf. Sci. 109–110 (1997) 249.
[14] A. Trovarelli, Catal. Rev. Sci. Eng. 38 (1996) 439.
[15] P.L.J. Gunter, J.W. Niemantsverdriet, F.H. Riebeiro, G.A. Somorjai, Catal. Rev. Sci. Eng. 39 (1997) 77.
[16] R.K. Usmen, G.W. Graham, W.L.H. Watkins, R.M. Mc Cabe, Catal. Lett. 30 (1995) 53.
[17] B. Ernst, L. Hilaire, A. Kiennemann, Catal. Today 50 (1999) 413.
[18] A. Bensalem, F. Bozon-Verduraz, M. Delamar, G. Bugli, Appl. Catal. A: Gen. 121 (1995) 81.
[19] G. Avgouropoulos, T. Ioannides, H.K. Matralis, J. Batista, S. Hocevar, Catal. Lett. 73 (1) (2001) 33.
[20] M. Daturi, E. Finocchio, C. Binet, J.C. Lavalley, F. Fally, V. Perrichon, H. Vidal, N. Hickey, J. Kaspar, J. Phys. Chem. B 104 (2000) 9186.
[21] J. Kaspar, P. Fornasiero, M. Grazini, Catal. Today 50 (1999) 285.
[22] W. Shan, M. Luo, P. Ying, W. Shen, C. Li, Appl. Catal. A: Gen. 246 (2003) 1.
[23] T. Takeshita, W.E. Wallace, R.S. Craig, J. Catal. 44 (1976) 236.
[24] V.T.Y. Coon, T. Takeshita, W.E. Wallace, R.S. Craig, J. Phys. Chem. 80 (1976) 1878.
[25] J. Barrault, A. Alouche, V. Paul-Boncour, L. Hilaire, A. Percheron-Guegan, Appl. Catal. 46 (1989) 269.
[26] G. Wrobel, M.P. Sohier, A. D'Huysser, J.P. Bonnelle, J.P. Marcq, Appl. Catal. A: Gen. 101 (1993) 73.
[27] A.M. Diskin, R.H. Cunningham, R.M. Ormerod, Catal. Today 46 (1998) 147.
[28] G.A. El-Shobaky, M.M. Doheim, A.M. Ghozza, Radiat. Phys. Chem. 69 (2004) 31.
[29] M.A. Ermakova, D.Yu. Ermakov, S.V. Cherepanova, L.M. Plyasova, J. Phys. Chem. B 160 (2002) 11922.
[30] J.B. Wang, Y.L. Tai, W.P. Dow, T.J. Huang, Appl. Catal. A: Gen. 218 (2001) 69.
[31] T. Takeguchi, S.-N. Furukawa, M. Inoue, J. Catal. 202 (2001) 14.
[32] W. Curtis Conner Jr., G.M. Pajonk, S.J. Teichner, Adv. Catal. 34 (1986) 1.
[33] W. Curtis Conner Jr., J.L. Falconer, Chem. Rev. 95 (1995) 759.
[34] J.A. La Verne, L. Tandon, J. Phys. Chem. B 106 (2001) 9316.
[35] S.J. Tauster, S.C. Fung, R.T.K. Baker, J.A. Horsely, Science 211 (1981) 1121.
[36] E. Ramaroson, J.F. Tempere, M.F. Guilleux, F. Vergand, H. Roulet, G. Dufour, J. Chem. Soc. Faraday Trans. 88 (1992) 1211.
[37] V.R. Mastelaro, V. Briois, D.P.F. de Souza, C.L. Silva, J. Ceram. Soc. 23 (2003) 273.
[38] M.P. Sohier, G. Wrobel, J.P. Bronnelle, J.P. Marcq, Appl. Catal. Gen. 84 (1992) 169.
[39] A. Roustila, C. Severac, J. Chêne, A. Percheron-Guégan, Surf. Sci. 311 (1994) 33.